

High Temperature Jahn-Teller Distortion and Short Range Order in CsCuCl₃

Emma A. Pappas,^{1,2} Toby Woods,³ Jue Liu,⁴ and Daniel P. Shoemaker^{1,2,5,*}

¹*Department of Physics, University of Illinois Urbana-Champaign, Urbana, IL, 61801, USA*

²*Materials Research Laboratory, University of Illinois at Urbana-Champaign, Urbana, IL, 61801, USA*

³*School of Chemical Sciences, University of Illinois Urbana-Champaign, Urbana, IL, 61801, USA*

⁴*Neutron Scattering Division, Oak Ridge National Laboratory, Oak Ridge, Tennessee 37831, United States*

⁵*Department of Materials Science and Engineering,
University of Illinois Urbana-Champaign, Urbana, IL, 61801, USA*

Abstract

CsCuCl₃, chiral and Jahn-Teller distorted at room temperature, takes a more symmetric structure above 423K. Describing this 'simpler' high temperature structure is far from simple and has been the subject of many, sometimes contradicting, studies. Here we reinvestigate the high temperature structure of CsCuCl₃, its thermal stability, and its effect on room temperature chirality. *In situ* pair distribution function data from powder neutron diffraction confirms that CsCuCl₃ is Jahn-Teller distorted both below and above T_c, and provides a quantitative view of short range order in the high temperature structure. *In situ* powder x-ray diffraction shows that CsCuCl₃ does not undergo any additional structural changes above 423K and is congruently melting. *In situ* single crystal x-ray diffraction experiments reveal that the phase transition induces domains of mixed handedness in originally homochiral crystals. These findings contribute to a better understanding of phase transitions in Jahn-Teller distorted compounds, and highlight the potential use of phase transitions to control chiral domains.

I. INTRODUCTION

At room temperature, CsCuCl₃ has a chiral P6₁22 or P6₅22 structure with helices of Jahn-Teller distorted CuCl₆ octahedra along the c-axis.¹ Around 423K, it undergoes a structural phase transition to a more symmetric, but probably still Jahn-Teller distorted structure, which has been the subject of many studies.

The structural phase transition of CsCuCl₃ was first discovered in 1971 by Natarajan and Prakash,² and by Kroese *et al.*³ They investigated the transition using differential thermal analysis, x-ray crystallography, and dielectric constant measurements. Their publications reported different high temperature crystal structures (cubic versus hexagonal), but both indicated that the transition is of first order, which was later confirmed by other studies on the electrical, optical, and thermal expansion properties.⁴⁻⁶

In 1974, Kroese *et al.* reassessed the high temperature structure using single crystal x-ray diffraction.⁷ They reported a hexagonal polar structure with space group P6₃mc. In their model, the Cu²⁺ ion is displaced along the c-axis, away from the center of the surrounding chlorine octahedron, resulting in a ferroelectric structure. The chlorine ions also has some anisotropic thermal motion along the c-axis. Kroese and Maaskant continued their study of the phase transition by assuming an idealized high temperature structure in the space group P6₃/mmc. They found a softening vibration mode at $k=(0,0,2\pi/3c)$.⁸

In 1975 and 1977, Hirotsu^{5,9} also showed that the $k=\pm(0,0,2\pi/3c)$ phonon mode relates the high and low

temperature phases and investigated the optical properties of CsCuCl₃ around the phase transition. They found that the optical rotation is not recovered upon heating and cooling and proposed that the transition induces enantiomorphic domains smaller than those originally present in the pristine crystal.⁵

In 1981, many publications introduced new information about the high temperature structure, contradicting or nuancing the results of previous studies. The far-infrared and Raman spectroscopy experiments of Petzelt *et al.* showed that, above the phase transition, CsCuCl₃ is non-polar with a high degree of disorder.¹⁰ They found that the phase transition has a soft mode with an infrared-active phason component. Crama redetermined the high temperature structure from single crystal x-ray diffraction experiments.¹¹ Multiple models taking into account the presence of a local Jahn-Teller effect were considered. The model with 3 split chlorine sites was determined to be the most probable and no softening of the $k=\pm(0,0,2\pi/3c)$ mode was found. Electron paramagnetic resonance (EPR) studies by Tanaka *et al.* suggested that static local distortions persist in the high temperature phase along with long-range intra-chain correlations.¹² Intra- and inter-chain interactions are also discussed in other works.^{13,14}

In 1985, Tanaka *et al.* conducted additional EPR experiments.¹⁵ They once again proposed that the CuCl₆ octahedra are Jahn-Teller distorted at high temperatures and showed that the distortions have long relaxation times. In 1986, Haije and Maaskant did magnetic susceptibility measurements on centimeter size crystals.¹⁶ They observed a transition from a static Jahn-Teller effect to a cooperative dynamic Jahn-Teller effect occurring in domains. That same year, Graf *et al.* performed neutron scattering experiments showing that the diffuse scatter-

* dpshoema@illinois.edu

ing at high temperature is incompatible with intra-chain correlations and can be interpreted as dense impurity Huang scattering.¹⁷ In 1987, Schotte showed that the neutron diffraction diffuse scattering was not due to short range correlations.¹⁸ The dense Huang scattering theory was continued in 1988 by Schotte *et al.*¹⁹ Additional neutron scattering experiments and theoretical work were done by Graf *et al.* in 1989.²⁰ They suggested that the first-order order-disorder transition could be triggered by an evolving second-order displacive transition far below the observed transition temperature. In 1997, another neutron experiment by Förster *et al.* saw some phonon softening at small q -values.²¹

Many other works have investigated the properties and phase transition of CsCuCl₃. For example, Maaskant and Haijie (1986) and Maaskant (1995) discussed the phenomenon of structural resonance,^{22,23} and Fernández *et al.* (1976), Vasudevan *et al.* (1979), and Bazán *et al.* (2009) reported additional high temperature phase transitions seen in measurements such as differential thermal analysis and differential scanning calorimetry.^{24–26}

It is easy to see that the research on CsCuCl₃ contains many contradictions. The non-polarity of the high temperature structure, the presence of soft modes and intra-chain correlations, and the nature of the first-order transition have all been questioned. Our work aims to clarify certain assertions about CsCuCl₃. In this paper, we re-investigate the high temperature structure of CsCuCl₃, its thermal stability, and the effect of the phase transition on chirality. First, we present new temperature dependent pair distribution function data from powder neutron diffraction. Our results confirm that CsCuCl₃ is Jahn-Teller distorted above the phase transition and show for the first time evidence of short range correlations. Second, we use *in situ* powder x-ray diffraction to search for additional structural phase transitions. No additional structural phase transitions are found up to the melting point of the compound. Third, we use *in situ* and *ex situ* single crystal x-ray diffraction to show that the phase transition induces chiral domains.

II. METHODS

A. Synthesis of CsCuCl₃

Single crystals of CsCuCl₃ are obtained by aqueous precipitation from solutions containing CuCl₂ and CsCl. Various synthesis conditions have been reported in the literature and it is often mentioned that an excess of CuCl₂ is needed to avoid the precipitation of Cs₂CuCl₄.^{27–31} We used crystals from three different batches of precipitation for our measurements. Each solution was prepared using granular powders of CuCl₂ (99% Acros) and CsCl (99.9% Sigma Aldrich) dissolved in deionized water with a 2:1 molar concentration. The solutions were filtered and left to evaporate for a few days to a few weeks in partially covered petri dishes or

beakers. Evaporation occurred at room temperature on a benchtop or in a fumehood. Crystals were rinsed with ethanol or deionized water before being used for measurements. Additional synthesis details for the crystals used in our measurements are available in the Supporting Information.

We performed other precipitations with various precursor concentrations and temperatures, and with and without filtering, seed crystals and surfactants. All synthesis conditions resulted in the precipitation of CsCuCl₃, as confirmed by powder x-ray diffraction, although some reactions also precipitated Cs₃Cu₃Cl₈OH.³² None of our reactions precipitated Cs₂CuCl₄. The morphology of our black CsCuCl₃ crystals is reminiscent of a rugby ball and reflection x-ray diffraction indicated that the long axis is the c -axis, in agreement with Soboleva *et al.* and Cui *et al.*^{33,34} We sometimes noticed liquid inclusions in certain crystals, which was also reported by Tanaka *et al.*¹⁵ Additional observations about the results of our various precipitation experiments can be found in the Supporting Information.

B. Sample Characterization and Measurements

Portions of the samples were crushed and analyzed using powder x-ray diffraction (PXRD) on a Bruker D8 diffractometer with a Mo x-ray source in transmission geometry. The sample for the *in situ* PXRD measurements was diluted with ground quartz before being sealed in an evacuated quartz capillary. The heating rate was 60 °C/min. The fixed temperature scans lasted 93 minutes and were preceded by a 7-minute hold. The crystal structures were refined using the Rietveld method with GSAS-II.³⁵ Representative fits to the PXRD data are available in the Supporting Information.

The chemical composition of some of the samples was analyzed using a scanning electron microscope (SEM) with energy dispersive x-ray spectroscopy (EDS). Representative results can be found in the Supporting Information along with details about the measurements.

Temperature dependent neutron diffraction and pair distribution function (PDF) data were collected at the NOMAD instrument at Oak Ridge National Laboratory.^{36,37} Two samples of CsCuCl₃ were measured and gave very similar data, so only one dataset is presented in this paper. Approximately 250 mg of powdered CsCuCl₃ was loaded into a 3 mm diameter thin-walled quartz capillary. An Oxford Instruments argon cryostream was used for temperature control. The sample was first cooled to 100 K and then heated to the target temperature at a rate of 6 K/min, where it was equilibrated for 5 min prior to data collection. At each temperature point, two 24 min scans were collected and summed to improve counting statistics. The diffraction data were background-subtracted using scattering data collected from an empty quartz capillary at the corresponding temperatures. The resulting scattering signals

were then normalized to the scattering from a 6 mm diameter vanadium rod to correct for detector efficiency. A second-order polynomial function was used to empirically model the Placzek correction and obtain the arbitrarily normalized total scattering function, $S(Q)$. A sine Fourier transform was then performed using a Q_{max} cutoff of 25 \AA^{-1} . Fourier filtering was applied to remove contributions from uncorrected multiple and inelastic scattering. A near-absolute $g(r)$ was obtained by fine-tuning the atomic number density such that $g(r)$ approached zero for interatomic distances smaller than 2 \AA . The reduced data $G(r) = 4\pi r \rho_0(g(r)-1)$ was fitted using PDFgui.³⁸ Values for Q_{damp} and Q_{broad} were obtained from fitting calibration data collected on silicon at 300 K. The calibration data was Fourier transformed using a Q_{max} cutoff of 40 \AA^{-1} and $G(r)$ was fitted from 0.5 to 50 \AA . The CsCuCl_3 PDF data was fitted from 0.5 to 20 \AA . In each fit, the data scale factor and delta1 (for data at 400 K, 450 K and 500 K) or delta2 (for data at 100 K and 300 K) were refined. The refinement conditions for the lattice parameters, atom positions, and thermal displacement parameters are specified in the discussion.

Differential scanning calorimetry (DSC) measurements were made on a Waters TA Instruments Discovery 2500 Differential Scanning Calorimeter. A few small crystals (approximately 50 mg) were placed in pressed aluminum pans and heated to $300 \text{ }^\circ\text{C}$ at a rate of $10 \text{ }^\circ\text{C}/\text{min}$. The measurement was performed on heating, cooling, and heating again, and was repeated on a second sample of similar mass.

Fragments of CsCuCl_3 crystals were used for single crystal x-ray diffraction (SCXRD). Intensity data were collected on a Bruker D8 Venture kappa diffractometer equipped with a Photon II (for the room temperature experiments) or Photon III (for the *in situ* experiments) CPAD detector. An $I\mu\text{s}$ microfocus source provided the $\text{Mo K}\alpha$ radiation ($\lambda = 0.71073 \text{ \AA}$) that was monochromated with multilayer mirrors. The sample was mounted on a 0.3 mm nylon loop with the minimal amount of Paratone-N oil. Data was collected as a series of ϕ and/or ω scans. For the *in situ* experiments, temperature control was achieved using a stream of $\text{N}_2(\text{g})$ provided by an Oxford Cryosystems Cryostream 1000. Initial data collection was performed at 298 K. The crystal was subsequently heated at 150 K/hr to 450 K. A 15 minute hold time at 450 K was used prior to commencement of data collection at 450 K. Upon completion of data collection at 450 K, the crystal was cooled at 150 K/hr back to 298 K. Following a 15 minute hold, a post-heating data set was collected at 298 K. The collection, cell refinement, and integration of intensity data was carried out with the APEX3 (room temperature) or APEX5 (*in situ*) software.³⁹ The absorption corrections were performed by multi-scan methods using SADABS.⁴⁰ The structures were solved with dual space methods using SHELXT version 2018/2.⁴¹ The structures were refined with the full-matrix least-squares routine of SHELXL version 2019/3.⁴² Data collection at a given temperature

took approximately 15 minutes.

The crystal structure drawings were produced with VESTA.⁴³

III. RESULTS AND DISCUSSION

A. Pair Distribution Function Analysis: Local Structure of CsCuCl_3

Below $150 \text{ }^\circ\text{C}$, CsCuCl_3 crystallizes in the P6_122 or P6_522 enantiomorphous structure pair. The chiral nature of the structures is noticeable in the positions of the cesium and copper ions, which form helices along the c -axis (see Fig.1(a)-(b)). The helix formed by the copper ions in the P6_122 structure is highlighted in orange in Fig.1(a). The chlorine ions form Jahn-Teller distorted octahedra around the copper ions, giving rise to 4 short and 2 long Cu-Cl bonds of lengths $2.281(4) \text{ \AA}$, $2.354(4) \text{ \AA}$, and $2.776(4) \text{ \AA}$ (two bonds of each length per copper ion). At 423K, CsCuCl_3 undergoes a structural change to a lower symmetry structure. The low temperature structure has a unit cell 3 times longer along c than the high temperature structure.

Discrepancies in the literature indicate that previous studies have been unable to accurately describe the chlorine positions in the high temperature phase. Two models have been proposed: a disordered $\text{P6}_3\text{mc}$ structure⁷ and a split-site $\text{P6}_3/\text{mmc}$ structure.¹¹ Both models are achiral as can be seen by the absence of the Cs and Cu spirals found in the low temperature chiral structure (see Fig.1(a),(d),(g)). The $\text{P6}_3\text{mc}$ structure, shown in Fig.1(d)-(f), reports large thermal ellipsoids to account for the uncertainty in the Cl positions. In this average structure, each copper ion makes 3 Cu-Cl bonds of 2.39 \AA and 3 Cu-Cl bonds of 2.51 \AA . The $\text{P6}_3/\text{mmc}$ structure, seen in Fig.1(g)-(i), places the Cl ions at 3 possible positions with equal probability to try to account for the presence of a local Jahn-Teller distortion. These split-sites give rise to possible Cu-Cl bond distances of 2.3300 \AA , 2.3606 \AA or 2.7221 \AA .

To investigate the local structure of the high temperature phase, we collected pair distribution function (PDF) data at 100K, 300K, 400K, 450K and 500K (see Fig.2). The data at 100K, 300K and 400K, below the 423K structural transition, display similar features, which broaden as the temperature increases due to thermal vibrations. At 450K and 500K, the peaks around 2.5, 7.5, 11.5 and 17.5 \AA have different intensity profiles compared to the low temperature data. These differences highlight the fact that the material has undergone a structural change. A feature of interest is the tall first peak and its smaller shoulder peak between 2 and 3 \AA , present at all temperatures. For every CsCuCl_3 structure, this length scale corresponds to the Cu-Cl bonds (see the bond contributions to the fit in Fig.3,4,5). At low temperature, this feature is explained by the 4 short and 2 long Cu-Cl bonds created by the Jahn-Teller distortion. The fact that this feature

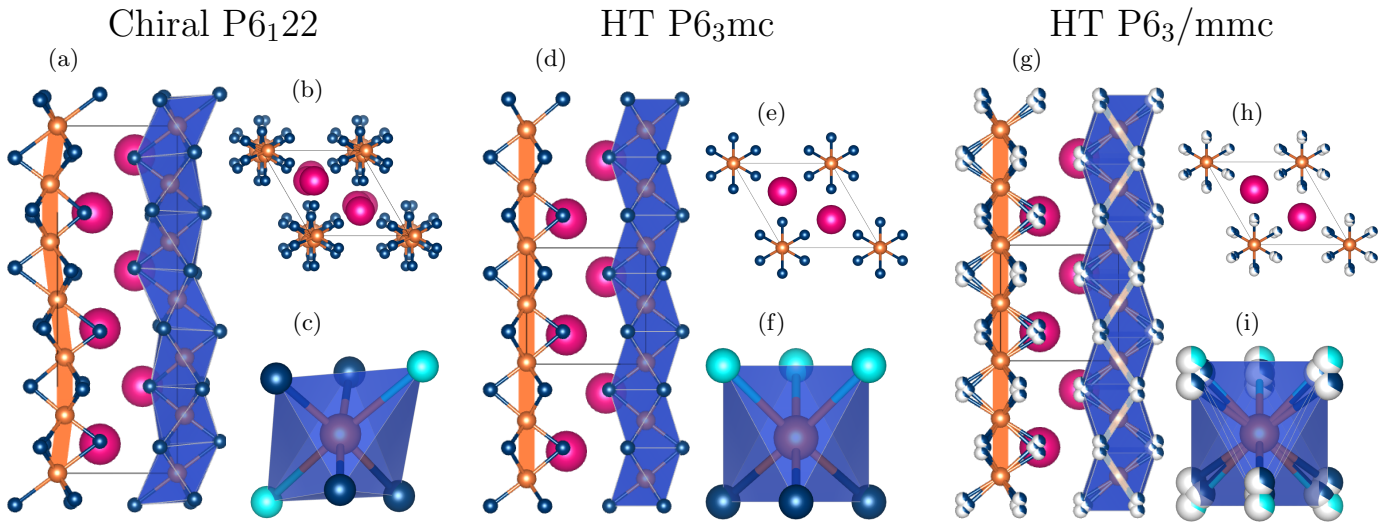


FIG. 1. Crystal structures of CsCuCl_3 with the Cs, Cu and Cl atoms in pink, orange and blue, respectively. Black lines outline single unit cells. (a)-(c) Room temperature $P6_122$ structure, (d)-(f) High temperature disordered $P6_3mc$ structure, (g)-(i) High temperature split-site $P6_3/mmc$ structure. Views of the structures along the a -axis are shown in (a), (d) and (g). The CuCl_6 octahedra are displayed on the right half of the structures. On the left half, orange highlights emphasize the Cu spiral found in the chiral $P6_122$ structure, but absent from the achiral $P6_3mc$ and $P6_3/mmc$ structures. Views of the structures along the c -axis are shown in (b), (e) and (h). In (c), (f) and (i), individual CuCl_6 octahedra are shown. Cu-Cl bonds 2.5 Å and longer are marked by light blue copper ions.

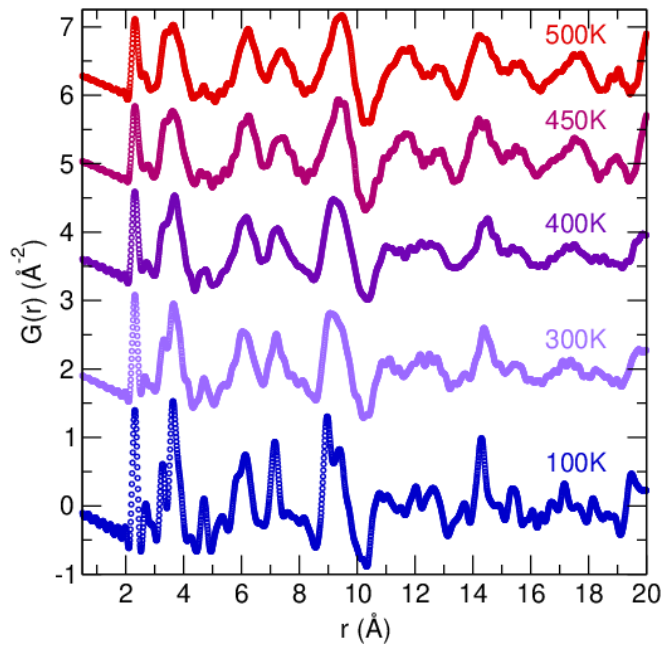


FIG. 2. Pair distribution function data collected on CsCuCl_3 at various temperatures. Below 423K, the sample is in the low temperature chiral structure, while above 423K, the sample takes an achiral structure.

persists in the 450K and 500K datasets is a first indication that the CuCl_6 octahedra are Jahn-Teller distorted even at high temperatures.

As expected, the $P6_122$ structure is a good fit to the

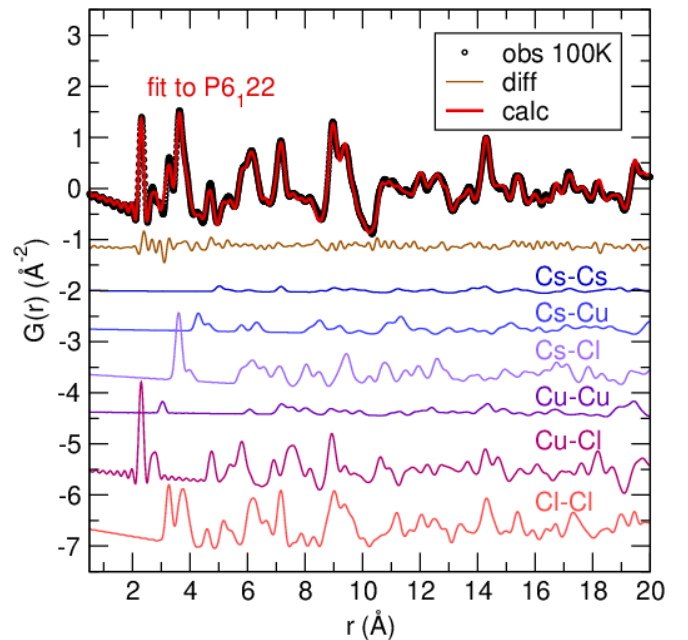


FIG. 3. The $P6_122$ structure of CsCuCl_3 is fitted (red curve) to the PDF data at 100K (black circles). The residuals (brown) and the contributions of each bond to the fit (labeled) are displayed below the fitted data.

pair distribution function data collected at 100K, 300K and 400K, which is below the structural transition at 423K. Fig.3 shows the fit at 100K. All fits of the $P6_122$ structure to the low temperature data have small resid-

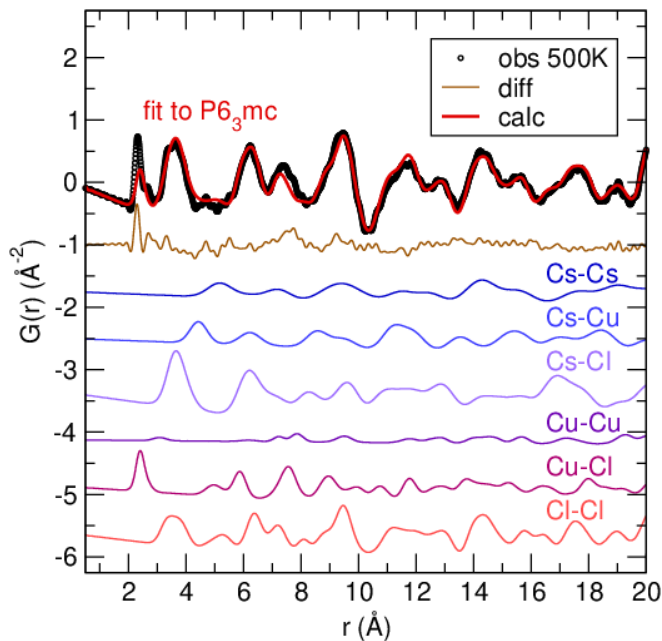


FIG. 4. The disordered $P6_3mc$ structure of $CsCuCl_3$ is fitted (red curve) to the PDF data at 500K (black circles). The residuals (brown) and the contributions of each bond to the fit (labeled) are displayed below the fitted data.

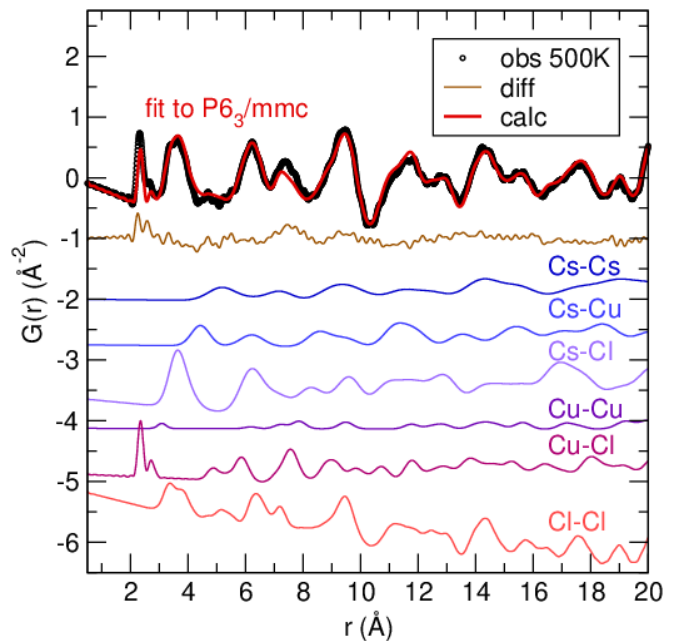


FIG. 5. The split-site $P6_3/mmc$ structure of $CsCuCl_3$ is fitted (red curve) to the PDF data at 500K (black circles). The residuals (brown) and the contributions of each bond to the fit (labeled) are displayed below the fitted data.

uals and weighted R-values between 0.10 and 0.15.

Fits of the disordered $P6_3mc$ and split-site $P6_3/mmc$ models to the 500K data are shown in Fig.4 and Fig.5. Fits of the 450K data give similar results. For both models, the lattice parameters and atomic displacement parameters are constrained and refined by symmetry, while the atom positions known from single crystal diffraction data^{7,11} are not refined. To fit the $P6_3/mmc$ split-site structure, we use a $2 \times 2 \times 2$ supercell with random chlorine site selection. Both models result in mis-fits of the first peak, its shoulder and the peak around 7.5 Å. Bond contributions indicate that these problems are mostly associated with the Cu-Cl and Cl-Cl bond distances. The disordered $P6_3mc$ model is a particularly poor match to the data between 2 and 3 Å. Its unique Cl site gives rise to too-similar Cu-Cl bond lengths of 2.39 Å and 2.51 Å creating a single broad peak instead of two. The poor fit of the $P6_3mc$ structure is to be expected, since it does not model the Jahn-Teller distortion visible in the data. The split Cl sites of $P6_3/mmc$ result in a slightly better fit, as the possible Cu-Cl distances of 2.3300 Å, 2.3606 Å or 2.7221 Å create the required two peaks between 2 and 3 Å. However, both high temperature models display significant misfits at short ranges and only adequately fit the data at long ranges. This shows that both models are representations of the average high temperature structure and incorrectly describe the precise positions of the chlorine ions. It is rather surprising that the $P6_3/mmc$ structure is such a poor fit at short ranges considering that the split-sites attempt to take into account the presence of a Jahn-Teller distortion at high temperature.

B. Pair Distribution Function Analysis: Short Range Ordering

To confirm that Jahn-Teller distorted $CuCl_6$ octahedra accurately describe the local high temperature structure and to verify the existence of a short range order, we fit the $CsCuCl_3$ room temperature structure over different ranges of r . Fits are performed in the range $r=0.5$ Å to r_{max} , where r_{max} varies from 5 to 20 Å by steps of 1 Å. The atom positions of the room temperature structure are refined and constrained by symmetry. To reduce the number of free parameters, we consider one isotropic thermal displacement parameter per element. We also fix the lattice parameters of all r_{max} fits to the values obtained for $r_{max}=20$ Å. The fits were sometimes sensitive to the initial guesses for the refined parameters, so for consistency, the initial guesses for a fit at $r_{max}=r$ are the results of the fit at $r_{max}=r+1$. Fits at different r_{max} values are performed on all datasets for comparison purposes.

Fits with low r_{max} values are only influenced by short range structural information. As r_{max} increases, information about the long range structure increases and the fits have to accommodate both the local and average structures, which differ at high temperatures due to the lack of long range order. The resulting atom positions should then gradually tend to those of the average structure, given by the $P6_3mc$ or $P6_3/mmc$ model. A similar procedure has been employed to demonstrate the presence of local order in $LaMnO_3$.⁴⁴

Fig.6 shows the Cu-Cl bond distances obtained when

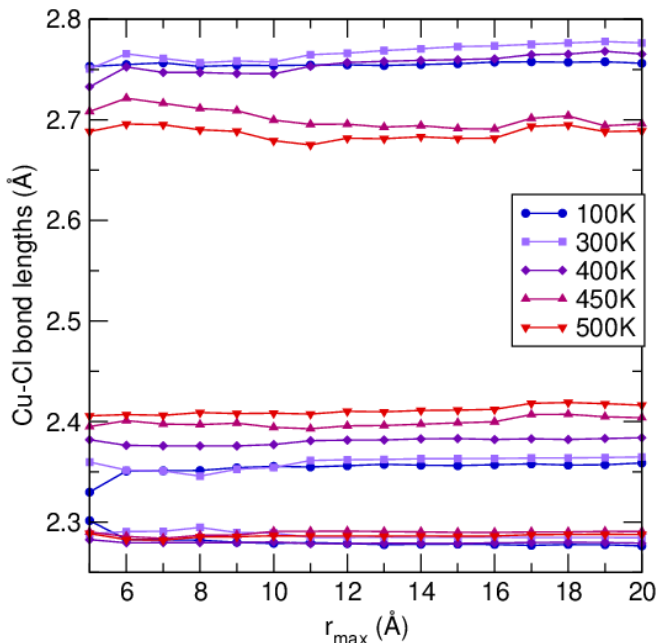


FIG. 6. Length of the three unique Cu-Cl bonds as the $P6_122$ structure is fitted to PDF datasets with different r_{max} cut-off. Fitted values for datasets at 100K, 300K, 400K, 450K and 500K are shown with blue circles, lilac squares, purple diamonds, burgundy up triangles and red down triangles, respectively.

fitting the room temperature Jahn-Teller distorted structure to the 100K, 300K, 400K, 450K and 500K datasets over different ranges of r . The 3 unique bonds of the $P6_122$ model are plotted (each bond occurs twice per CuCl_6 octahedra for a total of 6 bonds). For all temperatures and all r_{max} , the fits indicate the presence of 4 short and 2 long bonds. In particular, the shortest Cu-Cl bond takes a constant value at all temperatures, close to the reported room temperature value of $2.281(4) \text{ \AA}$.¹ This explains why the shortest Cu-Cl bond of the $P6_3/mmc$ split-site structure (2.3300 \AA)¹¹ poorly fits the PDF data. The second shortest Cu-Cl bond gets longer as the temperature increases. At 450K and 500K, it is longer ($\sim 2.4 \text{ \AA}$) than those reported by the room temperature $P6_122$ structure ($2.354(4) \text{ \AA}$) and by the high temperature $P6_3/mmc$ structure (2.3606 \AA). The $P6_3/mmc$ split-site structure also slightly overestimates the longest Cu-Cl bond (2.7221 \AA instead of $\lesssim 2.7 \text{ \AA}$).

The robust Cu-Cl distances over short and long ranges serve to confirm what we already knew from qualitative observations of the low- r PDF data and from the misfits of the $P6_3mc$ and $P6_3/mmc$ models; the Jahn-Teller distortions of the CuCl_6 octahedra persist at all temperatures. Below the phase transition, the long axes of the CuCl_6 octahedra form an ordered chiral motif along the c -axis. Above the phase transition, the average $P6_3mc$ or $P6_3/mmc$ structures are plausible average approximations because the orientations of the octahedra long axes become uncorrelated over long ranges. Octahedra may

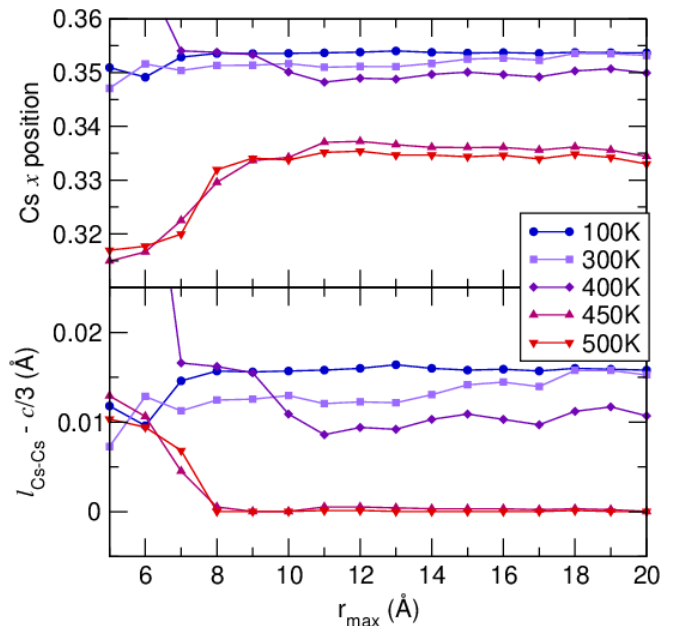


FIG. 7. Cesium positional parameters obtained from fitting the $P6_122$ structure on the 100K (blue circles), 300K (lilac squares), 400K (purple diamonds), 450K (burgundy up triangles) and 500K (red down triangles) PDF datasets with varying r_{max} . Top: x coordinate of the Cs atom at position $(x, 2x, 1/4)$. Bottom: Difference between the out-of-plane Cs-Cs bond length and one third of the c -axis length.

be uncorrelated from their immediate neighboring octahedra, or there may be ordered domains of few octahedra. Within those domains, the octahedra would be ordered, with the domains being orientationally disordered with respect to each other. To verify the existence of a short range order and determine its length scale, we take a closer look at the refined atom positions. The weighted R value of each fit is available in the Supporting Information, along with the refined values of the isotropic displacement parameters and $\delta 1$ or $\delta 2$.

1. Cs coordinates

In the $P6_122$ structure, the standard coordinate of the Cs ion is $(x, 2x, 1/4)$.¹ All other Cs coordinates can be obtained by symmetry and are thus defined by the value of x . In each unit cell, 3 Cs atoms are stacked along c . They have small in-plane displacements giving rise to the expected chiral motif (see Fig.1(d)-(e)). The out-of-plane Cs-Cs distances ($6.0767(4) \text{ \AA}$) are then larger than $1/3$ of the c -axis lattice parameter (6.0592 \AA).¹ The upper part of Fig.7 shows the refined value of x for different r_{max} , while the lower part shows the difference between this out-of-plane Cs-Cs bond length and $c/3$ for different values of r_{max} .

Fits for the 100K, 300K and 400K datasets result in almost perfectly constant x coordinate close to the re-

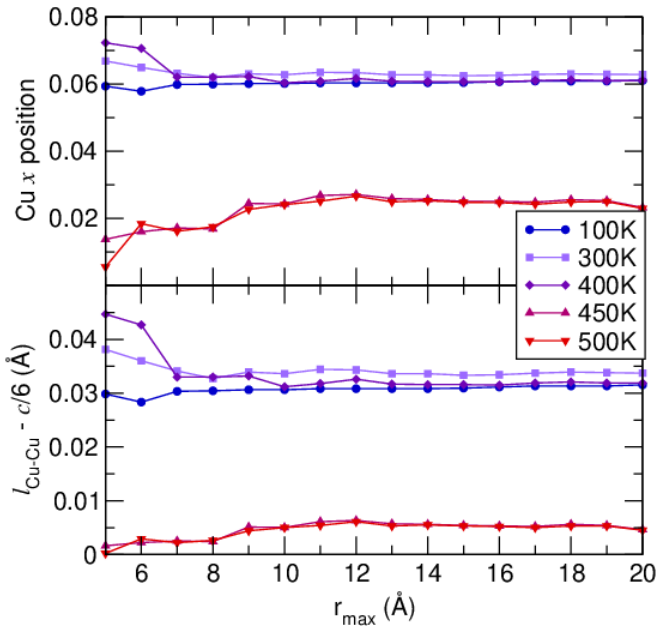


FIG. 8. Copper positional parameters obtained from fitting the $P6_122$ structure on the 100K (blue), 300K (lilac), 400K (purple), 450K (burgundy) and 500K (red) PDF datasets with varying r_{max} . Top: x coordinate of the Cu atom at position $(x, 0, 0)$. Bottom: Difference between the out-of-plane Cu-Cu bond length and one sixth of the c-axis length.

ported value of 0.35458.¹ The difference between the out-of-plane Cs-Cs bond length and $c/3$ is also constant and non-zero, as expected for the chiral phase. Two low r outliers in the 400K data are not shown in the figure and could be explained by the limited Cs bond information below 6 Å (the signal from the out-of-plane Cs-Cs bond is above 6 Å).

Fits for the 450K and 500K data show a very different trend than the low temperature data. For r_{max} less than 7 Å, x is close to 0.315, then it increases and plateaus to about 0.335. In both the $P6_3mc$ and the $P6_3/mmc$ structures, the standard Cs coordinate is $(1/3, 2/3, 3/4)$.^{7,11} At large r_{max} , the refined Cs x coordinate is then very close to that of the average structure. The plot of $l_{Cs-Cs} - c/3$ highlights that the change in coordinate occurs at $r_{max}=8$ Å. From $r_{max}=8$ to 20 Å, $l_{Cs-Cs} - c/3$ is zero, indicating that the cesium atoms take achiral positions. Below $r_{max}=8$ Å, the difference between the out-of-plane Cs-Cs bond length and $c/3$ is similar to that of the low temperature data. It is also interesting to note that the low temperature x coordinate and the small r_{max} high temperature x coordinate are almost equidistant from the average long range x coordinate at high temperature. This highlights the resemblance of the local high temperature structure with the low temperature structure.

2. Cu coordinates

In the $P6_122$ structure, the standard coordinate of the Cu ion is $(x, 0, 0)$ ¹ and all other Cu coordinates can be expressed in terms of x . The Cu atoms form spirals along the c-axis with 6 atoms per spiral per unit cell. The chiral motif induces a small in-plane displacement ($x \neq 0$) that makes the out-of-plane Cu-Cu bond lengths (3.0620(4) Å) longer than one sixth of the c-axis lattice parameter (3.0296 Å). The top and bottom portions of Fig.8 show the refined value of x and the length difference between the out-of-plane Cu-Cu bond and $c/6$ for different values of r_{max} . For 100K, 300K and 400K, both plots show constant positions and bond lengths at all r_{max} , with x close to the reported value of 0.06160.¹ Fluctuations at $r_{max}=5$ and 6 Å can be explained by the limited Cu bonding information.

At 450K and 500K, the values of x and of the bond length difference are smaller than at low temperatures. They increase slightly as r_{max} increases, up to about 9 Å, at which point the values stabilize and tend to approximately 0.02 for x and 0.005 for the length difference. In the $P6_3mc$ structure, the standard coordinate of the Cu ion is $(0, 0, z)$ with $z=0.015$, and in the $P6_3/mmc$ structure it is $(0, 0, 0)$.^{7,11} The average long range Cu positions given by the $P6_122$ fits are then close to those reported for the $P6_3mc$ and $P6_3/mmc$ structures.

3. Cl coordinates

The Cl ions of structure $P6_122$ are distributed over two different Wyckoff sites; 6b with standard coordinate $(x, 2x, 1/4)$, and 12c with standard coordinate (x, y, z) .¹ Fig.9 shows the fitted values of these four coordinates for different values of r_{max} and for the different temperature datasets. For 100K, 300K and 400K, all coordinates are constant as r_{max} increases and are very similar to the values found in the literature. For the 6b site, the reported value of x is 0.88770, and for the 12c site, the reported coordinate is (0.20950, 0.35400, 0.09153).¹ Multiple strong peaks for Cu-Cl and Cl-Cl bonds are present in the data for all ranges of r_{max} , so no fluctuations are seen in the low temperature small r_{max} fits.

At 450K and 500K, all coordinates are constant except for the x coordinate of the 12c site (second panel from the bottom in Fig.9). The value is lower than at low temperatures and it slightly increases before becoming constant at $r_{max}=9$ Å. The large r_{max} behavior indicates that the 6b Cl sites have an average position leading them further away from the nearest Cu atom (second shortest Cu-Cl bond in Fig.6), while the 12c Cl sites have an average position leading them closer to the nearest Cu atom (shortest and longest Cu-Cl bonds in Fig.6).

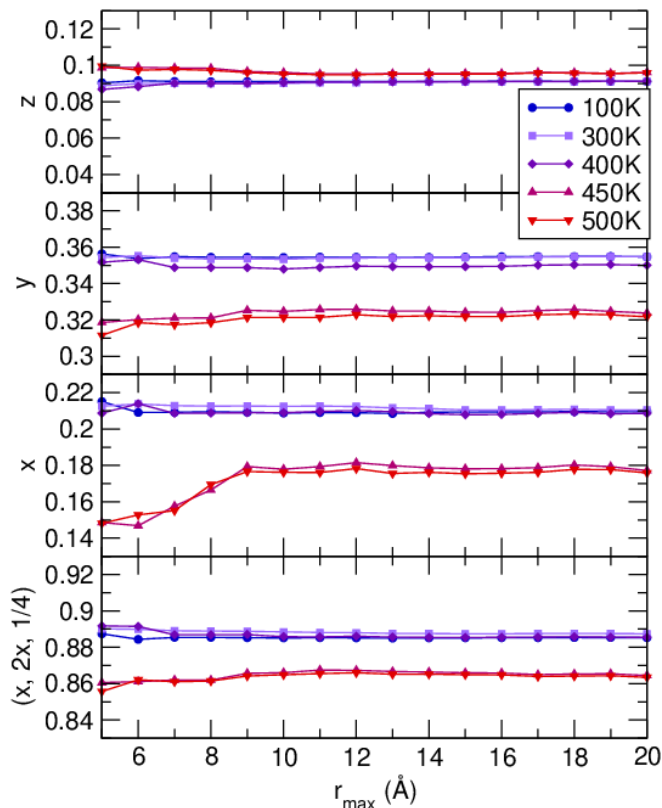


FIG. 9. Coordinates of the Cl atoms as the $P6_122$ structure is fitted to PDF datasets with different r_{max} cutoff. The bottom panel displays the value of x for the Wyckoff position 6b with coordinate $(x, 2x, 1/4)$, while the three top panels display the values of x , y and z for the Wyckoff position 12c. Fitted values for datasets at 100K, 300K, 400K, 450K and 500K are shown with blue circles, lavender squares, purple diamonds, burgundy up triangles and red down triangles, respectively.

4. Short range correlation length

Correlation lengths can typically be obtained by small box least squares fitting⁴⁴ or by large box Monte Carlo modeling.⁴⁵ Here we used small box least square fitting to show that short range correlations are present in the high temperature phase of CsCuCl_3 and to estimate their length scale.

At 450K and 500K, the short and long range fits give different values for the Cs, Cu and Cl ion positions, indicating the presence of short range correlations. The change in values occurs around 8 or 9 Å. This suggests that the Jahn-Teller distorted CuCl_6 octahedra are ordered over domains of length 8-9 Å. It is interesting to note that this corresponds to a length of approximately 3 CuCl_6 octahedra (9.186 Å).

Another fitting scheme to search for short range correlations was explored: $P6_3mc$ supercells with unconstrained atom positions. The details and results of which are available in the Supporting Information. These additional fits also support the claim that correlations occur

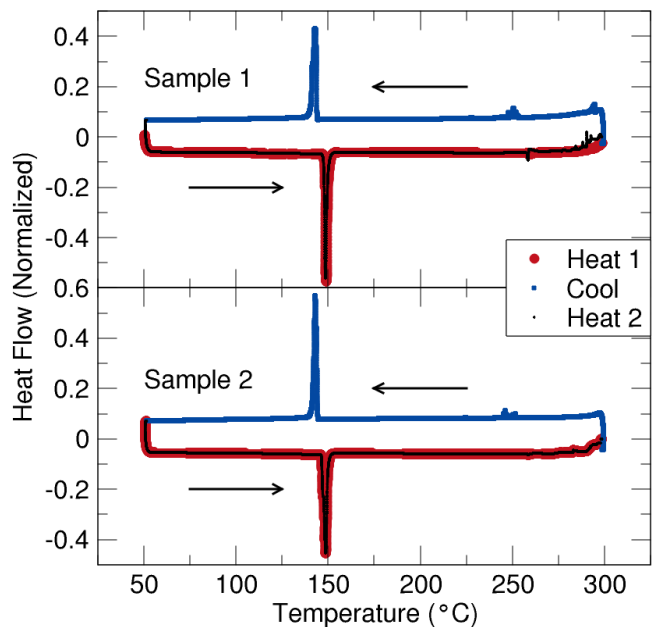


FIG. 10. Differential scanning calorimetry (DSC) data collected on two samples of CsCuCl_3 . The samples were heated (red thick line), cooled (blue line), and heated again (black thin line). Arrows indicate the direction of heating/cooling. The structural phase transition occurred at 149 °C on heating and at 143 °C on cooling.

over 3 CuCl_6 octahedra.

In 1986, Graf *et al.* stated that the position and change of the diffuse scattering observed in neutron diffraction data indicated that no intra-chain correlations exist in the high temperature phase of CsCuCl_3 .¹⁷ In 1987, Schotte compared the shape of the diffuse scattering to simulated data and concluded that there are no short range correlations in specific crystallographic directions.¹⁸ Our results are in disagreement with these studies as we see clear evidence of short range correlations on the order of 8 to 9 Å.

C. Stability of CsCuCl_3 by diffraction and calorimetry

While the presence of a structural transition at 423K in CsCuCl_3 is widely accepted, other unspecified transitions have been detected in previous studies. For example, Fernández *et al.* report additional transitions at 511K and 535K as seen by differential thermal analysis.²⁴ Vasudevan *et al.* and Bázan *et al.* also observed these transitions by far infrared spectroscopy and differential thermal analysis, respectively.^{25,26} We did not observe these transitions in our differential scanning calorimetry (DSC) measurements (see Fig.10) and we observed no structural changes above 200 °C as indicated by our *in situ* powder x-ray diffraction (PXRD) data (see Fig.11). We think that the small signals previously seen at 511K

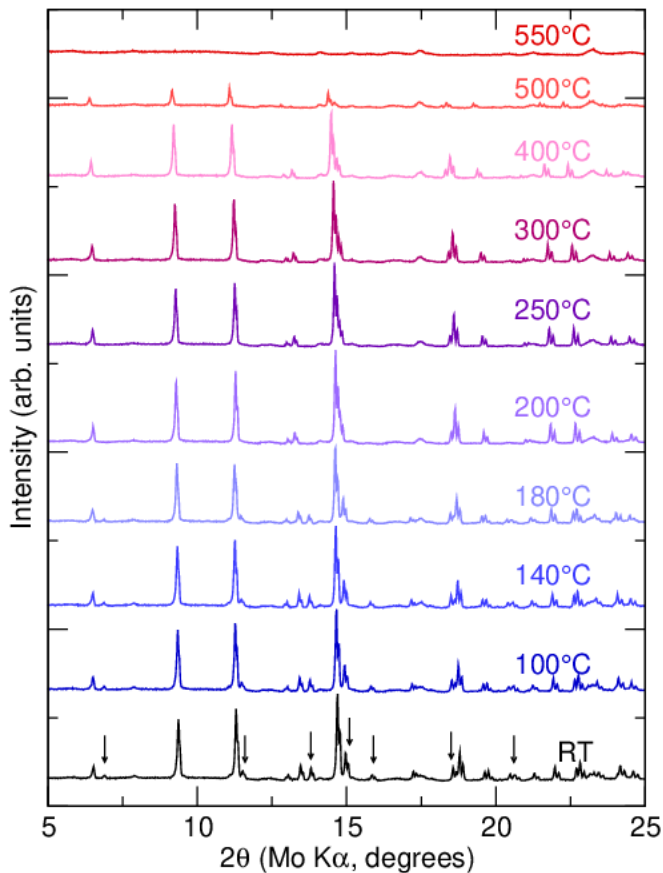


FIG. 11. *In situ* powder x-ray diffraction of CsCuCl_3 collected on heating. Because of furnace insulation effects, the structural phase transition happens between 180 °C and 200 °C, instead of 150 °C. Subtle changes in the peak profiles and intensities are signs of the phase transition; the relevant peaks are marked by black arrows in the room temperature data.

and 535K are from liquid inclusions or minor phase impurities.

DSC data was collected on two different samples, twice on heating and once on cooling. Our DSC data shows a phase transition at 149 °C on heating and 143 °C on cooling, which is in good agreement with the reported value of 150 °C for the chiral-achiral phase transition. Having some amount of thermal hysteresis is also in agreement with previous reports.^{2,5,24} Some of our datasets have liquid inclusions in the CsCuCl_3 crystals. Crystals from the same batch of crystals used for the DSC measurements were heated above 300 °C and were found to “jump.” We suspect that some of the crystals from that batch may have liquid inclusions, which are suddenly expelled when the crystals are sufficiently heated. Some crystals from other synthesis procedures (not used for measurements in the present paper) were also found to have small liquid inclusions revealed by polishing. Based on our findings, we do not believe that CsCuCl_3 has any additional phase transitions above the structural change at 150 °C.

PXRD data collected on heating is shown in Fig.11

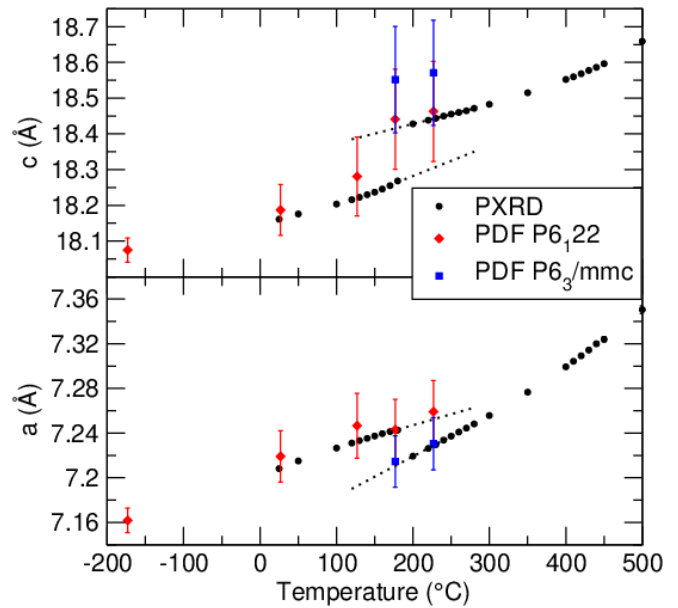


FIG. 12. Lattice parameters of CsCuCl_3 at different temperatures. Black circles indicate data obtained from fitting powder x-ray diffraction data with the $P6_122$ (25 to 180 °C) and $P6_3/mmc$ (200 to 500 °C) structures. Red diamonds and blue squares indicate data obtained from fitting the $P6_122$ or $P6_3/mmc$ structures, respectively, to pair distribution function data. Error bars are plotted, but are sometimes too small to be seen. Black dotted lines extrapolate the PXR data between 120 and 280 °C to highlight the change in the lattice parameters (0.4% contraction in a and 0.8% expansion in c).

for selected temperatures. A zoomed-in view of the 5 to 25° 2θ range is presented to better highlight the visual changes in the signal associated with the structural phase transition: a minuscule peak around 7° disappears, a shoulder peak around 11.5° disappears, a small peak around 14° disappears, two peaks around 15° start to merge, a small peak around 16° disappears, one of the two small peaks around 17° disappears, and a small peak around 20.5° disappears. These changes can be observed between the data at 180 °C and 200 °C, and the peaks in question are indicated by arrows in the room temperature dataset.

The PXR data shows that the chiral structure persisted up to 180 °C, which is above the reported transition temperature of 150 °C and the transition temperature we obtained from our DSC data. The discrepancy between these values can be attributed to insulation differences, with the DSC data giving a more precise and reliable value for the transition temperature. At 200 °C, the PXR data fits well to the high temperature achiral structure. No other structural changes are observed up to 500 °C, where a decrease in the signal indicates that the sample is starting to melt. Lack of signal at 550 °C indicates that the sample is completely melted. Comparison of data collected with and without the furnace indicate that minimal scattering from the furnace is

present, which is visible in the 550 °C dataset. On cooling (not shown), the signal reappears around 450 °C and increases in strength until about 300 °C. After 300 °C, further cooling does not increase the PXRD signal intensity. The room temperature PXRD data obtained after heating seems to indicate that the *in situ* sample is preferentially oriented CsCuCl₃.

To confirm that CsCuCl₃ is congruently melting, crystals from a different synthesis batch were ground to powder, sealed in an evacuated quartz tube, heated to 550 °C at 10 °C/min, held at 550 °C for 30 min, and slow cooled at 2.5 °C/min. This annealing melted the sample and PXRD confirmed that the sample was still CsCuCl₃. BASF (Batch Scale Factor) parameters obtained from single crystal x-ray diffraction on 3 fragments indicated that the sample was of mixed chirality after melting. Soboleva *et al.* reported that CsCuCl₃ melts and partially decomposes at 455 °C.³³ The reported melting temperature is in reasonable agreement with our *in situ* PXRD results. However, we did not observe any partial decomposition and found that CsCuCl₃ is congruently melting.

The PXRD data from 25 °C to 180 °C was fitted to the P6₁22 structure, while the PXRD data from 200 °C to 500 °C was fitted to the P6₃/mmc structure. Fits of the data at 25 °C, 200 °C and 400 °C are available in the Supporting Information. Values for the lattice parameters are plotted in Fig.12 along with the values obtained from fits of the PDF data. Since the low temperature P6₁22 structure has a c-axis that is about 3 times longer than that of the high temperature P6₃/mmc structure, the refined value of the high temperature c-axis is tripled in Fig.12. For the PDF data at 450K and 500K, the lattice parameters obtained from fits of the P6₁22 and P6₃/mmc structures are present (for fit details, see the description of the P6₁22 r_{max} fits and the description of the P6₃/mmc supercell fit in the previous sections). Fig.12 shows that there is a noticeable change in the lattice parameters at the phase transition. This change is at the correct temperature (150 °C) for the PDF data, but a temperature lag in the PXRD data artificially shifts the transition to a higher temperature. Black dotted lines show lattice parameter values extrapolated from the PXRD data between 120 and 180 °C and between 200 and 280 °C. These extrapolations indicate that the lattice undergoes a 0.4% contraction along *a* and a 0.8% expansion along *c* during the phase transition. Our results are in reasonable agreement with the dilatometry measurements of Hirotsu (1975).⁵

D. Absolute structure of pristine and heated CsCuCl₃

Many studies have reported that CsCuCl₃ crystals obtained by aqueous precipitation are heterochiral. Measurements of optical activity,⁵ single crystal x-ray diffraction (SCXRD) Flack parameters,^{31,46-48} anomalous x-ray scattering,²⁹ and resonant circularly polarized x-ray

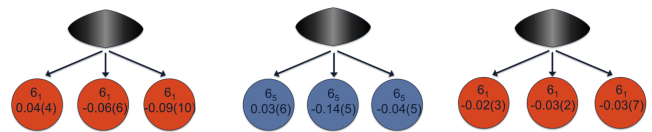


FIG. 13. Space groups and Flack parameters obtained from single crystal x-ray diffraction of pristine CsCuCl₃ crystals. Three fragments (colored disks) are measured from each of the three crystals (black rhombuses). Space groups P6₁22 (red) and P6₅22 (blue) are abbreviated by 61 and 65, respectively. Near zero Flack parameters indicate that all fragments are homochiral. Fragments taken from the same crystal have the same handedness, suggesting that the crystals are homochiral.

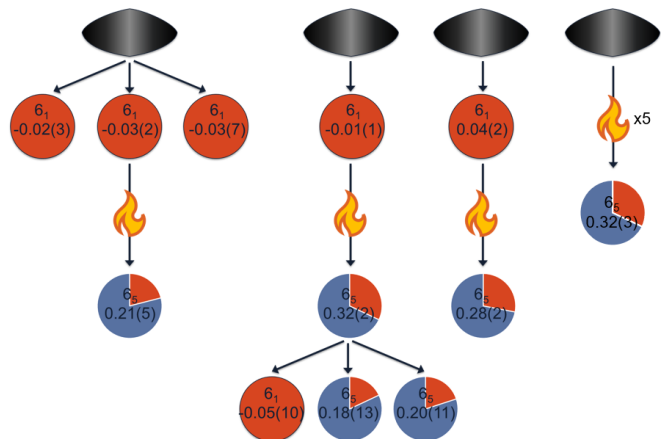


FIG. 14. Space groups and Flack parameters obtained from *in situ* and *ex situ* single crystal x-ray diffraction of fragments (colored pie charts) of CsCuCl₃ crystals (black rhombuses). Space groups P6₁22 (red) and P6₅22 (blue) are abbreviated by 61 and 65, respectively. Crystal fragments have near zero Flack parameters before being heated to 450K, indicating that they are homochiral at the start. After being heated and cooled through the phase transition (fire icon), the fragments are of mixed chirality. The last schematic to the right shows that a fragment taken from a crystal cycled 5 times through the phase transition is also heterochiral.

diffraction^{46,49} have shown that as grown crystals had domains of different chirality. Methods to obtain homochiral crystals have been found; stirring,³¹ heating⁴⁷ and adding certain organic solvents⁴⁸ to the solution lead to the precipitation of homochiral crystals (based on measurements of SCXRD Flack parameters). Homochiral seeds can then be used to obtain larger homochiral crystals.⁵⁰

In situ measurements of optical rotation⁵ also showed that the rotation angle, initially non-zero, becomes null after heating and cooling CsCuCl₃ through the phase transition. This result seemed to indicate that fine enantiomeric domains smaller than the probed region (1 mm) are forming as the low temperature structure is recovered.⁵

To verify the absolute structure of our as grown CsCuCl₃, we measured the SCXRD Flack parameters of

a few crystals from two different precipitation batches. Fig.13 shows the Flack parameter and space group of 9 fragments of pristine CsCuCl₃ taken from 3 different crystals. Near zero Flack parameters indicate that all fragments are homochiral. Fragments obtained from the same crystal also display the same handedness. This suggests that the CsCuCl₃ crystals in our study are homochiral, in contrast to the many studies reporting heterochiral as grown crystals of CsCuCl₃.^{5,29,31,46–49}

To verify the effects of the phase transition on the chirality of CsCuCl₃, we measured the Flack parameters of 3 fragments before and after heating to 450K and cooling back to room temperature. As seen in Fig.14, all 3 fragments, originally homochiral, are of mixed handedness after undergoing the phase transition. The dominant handedness is also changed by the heating and cooling. One heated fragment was broken in 3 pieces and the Flack parameter was measured again. Two of these smaller pieces are of mixed chirality and have an opposite dominant handedness compared to the third piece. The different results obtained for these 3 smaller pieces highlight again that the phase transition induces chiral domains. This result is also robust when we heat larger crystals, and not just small fragments. One crystal was heated and cooled through the phase transition 5 times before we measured the Flack parameter of a fragment. The measurement indicates that the crystal fragment is of mixed handedness, in contrast to the results of the pristine crystal fragments (see Fig.13). Larger crystals are seemingly unaffected by repeated temperature cycling and maintain their integrity and crystallinity. Our *in situ* single crystal XRD experiments are then in agreement with the results of the *in situ* optical rotation experiments by Hirotsu.⁵

IV. CONCLUSIONS

We reinvestigated the high temperature structure of CsCuCl₃ using pair distribution function analysis of neutron diffraction data. Our results show that the high temperature phase is Jahn-Teller distorted and that short range correlations exist on the order of 8-9 Å. To the best of our knowledge, this is the first evidence and characterization of the short range order in the high temperature structure of CsCuCl₃.

We used differential scanning calorimetry, *in situ* powder x-ray diffraction, and annealing experiments to investigate the thermal stability of CsCuCl₃. We found no additional structural phase transitions and confirmed that CsCuCl₃ is congruently melting. The phase transition at 150 °C leads to a 0.4% contraction of the unit cell along *a* and a 0.8% expansion along *c*.

Our single crystal x-ray diffraction experiments revealed that our as grown crystals are most likely homochiral, a surprising result in light of the many reports of as grown heterochiral crystals. More importantly, our experiments showed that the phase transition induces chiral domains in CsCuCl₃. This opens the door to new

methods of controlling chirality in polymorphic materials. A more detailed investigation of the impact of the phase transition on domain formation in CsCuCl₃ is underway. Results of our *in situ* chirality maps obtained by resonant circularly polarized x-ray diffraction will be available in an upcoming publication.

SUPPORTING INFORMATION

Additional synthesis details, powder XRD refinements, SEM-EDS images, and pair distribution function analysis.

ACKNOWLEDGMENTS

Preliminary work on this compound was supported by the Center for Quantum Sensing and Quantum Materials, an Energy Frontier Research Center funded by the U.S. Department of Energy, Office of Science, Basic Energy Sciences, under Award DE-SC0021238. Neutron scattering was performed at the Spallation Neutron Source (IPTS-36285), a DOE Office of Science User Facility operated by the Oak Ridge National Laboratory. Synthesis and characterization were carried out in the Materials Research Laboratory Central Research Facilities, University of Illinois. EAP was partially funded by a Ludo Frevel Crystallography Scholarship awarded by the International Centre for Diffraction Data.

REFERENCES

- 1 Albert W. Schlueter, Robert A. Jacobson, and Robert E. Rundle. A Redetermination of the Crystal Structure of CsCuCl₃. *Inorganic Chemistry*, 5(2):277–280, February 1966.
- 2 M. Natarajan and B. Prakash. Phase transitions in abx₃ type halides. *physica status solidi (a)*, 4(3):K167–K172, 1971.
- 3 C J Kroese. A PHASE TRANSITION IN A COMPOUND WITH HELICAL ELECTRIC DIPOLE STRUCTURE: CsCuCl₃.
- 4 R. Laiho, M. Natarajan, and M. Kaira. Some electrical and optical studies in cscucl3 crystals. *physica status solidi (a)*, 15(1):311–317, 1973.
- 5 S Hirotsu. Some optical and thermal properties of CsCuCl₃ and its phase transition near 423K. *Journal of Physics C: Solid State Physics*, 8(1):L12–L16, January 1975.
- 6 N. I. Sorokin. Electrical conductivity of CsCuCl₃ crystals at structural phase transition. *Crystallography Reports*, 62(4):629–631, July 2017.
- 7 C J Kroese. The High-Temperature Structure of CsClCl₃.
- 8 C. J. Kroese and W. J. A. Maaskant. The relation between the high-temperature and room-temperature structure of CsCuCl₃. *Chemical Physics*, 5(2):224–233, August 1974.
- 9 S Hirotsu. Jahn-Teller induced phase transition in CsCuCl₃ : structural phase transition with helical atomic

- displacements. *Journal of Physics C: Solid State Physics*, 10(7):967–985, April 1977.
- 10 J. Petzelt, I. Gregora, V. Vorlíček, J. Fousek, B. Březina, G. V. Kozlov, and A. A. Volkov. Far-infrared and Raman spectroscopy of the phase transition in CsCuCl_3 . *Journal of Raman Spectroscopy*, 10(1):187–193, January 1981.
 - 11 W. J. Crama. The Jahn–Teller distorted structure of caesium copper(II) trichloride. *Acta Crystallographica Section B: Structural Crystallography and Crystal Chemistry*, 37(12):2133–2136, December 1981.
 - 12 Hidekazu Tanaka, Katsunori Iio, and Kazukiyo Nagata. Influence of cooperative jahn-teller effect in CsCuCl_3 crystals on the broadening of epr lines. *Journal of the Physical Society of Japan*, 50(3):727–728, 1981.
 - 13 Yūichi Tazuke, Hidekazu Tanaka, Katsunori Iio, and Kazukiyo Nagata. Magnetic Susceptibility Study of CsCuCl_3 . *Journal of the Physical Society of Japan*, 50(12):3919–3924, December 1981.
 - 14 H Tanaka, H Dachs, K Iio, and K Nagata. Structural phase transitions in hexagonal ABC_3 Jahn-Teller crystals: I. Face-sharing coupling and ground-state configuration. *Journal of Physics C: Solid State Physics*, 19(25):4861–4878, September 1986.
 - 15 Hidekazu Tanaka, Katsunori Iio, and Kazukiyo Nagata. Electron Paramagnetic Resonance in the Quasi-One-Dimensional Jahn-Teller-Crystals. I. CsCuCl_3 . *Journal of the Physical Society of Japan*, 54(11):4345–4358, November 1985.
 - 16 W. G. Haije and W. J. A. Maaskant. A magnetic susceptibility study on the dynamic Jahn-Teller effects in CsCuCl_3 : single octahedron and cooperative phenomena. *Journal of Physics C: Solid State Physics*, 19(35):6943, December 1986.
 - 17 H. A. Graf, H. Tanaka, H. Dachs, N. Pyka, U. Schotte, and G. Shirane. Jahn-Teller phase transition in CsCuCl_3 and CsCrCl_3 : A neutron scattering study. *Solid State Communications*, 57(6):469–472, February 1986.
 - 18 U. Schotte. Theory of diffuse neutron scattering in the high temperature phase of CsCuCl_3 and related Jahn-Teller compounds. *Zeitschrift für Physik B Condensed Matter*, 66(1):91–101, March 1987.
 - 19 U. Schotte, H. A. Graf, and H. Dachs. Elastic dipole theory of CsCuCl_3 and related hexagonal Jahn-Teller compounds for neutron scattering. *Journal of Physics: Condensed Matter*, 1(24):3765, June 1989.
 - 20 H A Graf, G Shirane, U Schotte, H Dachs, N Pyka, and M Iizumi. Quasi-elastic and inelastic neutron scattering in the high temperature phase of the cooperative Jahn-Teller system CsCuCl_3 . *Journal of Physics: Condensed Matter*, 1(24):3743–3763, June 1989.
 - 21 U. Förster, H. A. Graf, U. Schotte, and U. Stuhr. Phonon renormalisation at small q values in the HT-phase of CsCuCl_3 . *Physica B: Condensed Matter*, 234-236:142–143, June 1997.
 - 22 W. J. A. Maaskant and W. G. Haije. On the Jahn-Teller-induced helical deformations in CsCuCl_3 . *Journal of Physics C: Solid State Physics*, 19(27):5295, September 1986.
 - 23 Wim J. A. Maaskant. On helices resulting from a cooperative Jahn-Teller effect in hexagonal perovskites. In *Iron-Sulfur Proteins Perovskites*, pages 55–87. Springer, Berlin, Heidelberg, 1995.
 - 24 J. Fernández, M.J. Tello, J. Peraza, and E.H. Bocanegra. New high temperature phase transitions in cesium cupric chloride. *Materials Research Bulletin*, 11(9):1161–1167, September 1976.
 - 25 JAHN—TELLER EFFECT INDUCED PHASE TRANSITIONS IN CsCuCl_3 Errata. *Physics Letters A*, 72(6):481, August 1979.
 - 26 Julio C. Bazán, Gabriela M. Lescano, María R. Prat, and Aurora Sagua. Reduction of Cu(II) to Cu(I) in solid CsCuCl_3 . *Materials Chemistry and Physics*, 125(3):542–547, February 2011.
 - 27 J. J. O’Connor, M. A. Dipietro, and A. F. Armington. Preparation and properties of cesium cupric chloride. *Journal of Crystal Growth*, 6(4):346–348, May 1970.
 - 28 Kimio Adachi, Norio Achiwa, and Mamoru Mekata. Helical Magnetic Structure in CsCuCl_3 . *Journal of the Physical Society of Japan*, 49(2):545–553, August 1980.
 - 29 T Koiso, K Yamamoto, Y Hata, Y Takahashi, E Kita, K Ohshima, and F P Okamura. Determination of the chiral structure of using anomalous x-ray scattering near the Cs K absorption edge. *Journal of Physics: Condensed Matter*, 8(38):7059, September 1996.
 - 30 L. V. Soboleva. Growth of functional single crystals of complex compounds on the basis of the solubility phase diagrams of ternary systems. *Crystallography Reports*, 53(1):164–170, January 2008.
 - 31 Yusuke Kousaka, Takemi Koyama, Marina Miyagawa, Kohei Tanaka, Jun Akimitsu, and Katsuya Inoue. Crystal Growth of Chiral Magnetic Material in CsCuCl_3 . *Journal of Physics: Conference Series*, 502:012019, April 2014.
 - 32 Natalija Van Well, Michael Bolte, Claudio Eisele, Lukas Keller, Jürg Schefer, and Sander Van Smaalen. Mixed system $\text{Cs}_3\text{Cu}_3\text{Cl}_8\text{-xBr}_x\text{OH}$ with weakly connected Cu-triangles. *Journal of Physics and Chemistry of Solids*, 140:109386, May 2020.
 - 33 L. V. Soboleva, I. M. Sil’vestrova, Z. B. Perekalina, A. B. Gil’varg, and Yu N. Martyshev. Investigation into some physical properties of the CsCuCl_3 crystal. 21(6):1140–1147, November 1976.
 - 34 Shuting Cui, Yan Chen, Siwen Tao, Jiawen Cui, Cang Yuan, Ning Yu, Huawei Zhou, Jie Yin, and Xianxi Zhang. Synthesis, Crystal Structure and Photoelectric Response of All-Inorganic Copper Halide Salts CsCuCl_3 . *European Journal of Inorganic Chemistry*, 2020(22):2165–2169, June 2020.
 - 35 Brian H. Toby and Robert B. Von Dreele. *GSAS-II*: the genesis of a modern open-source all purpose crystallography software package. *Journal of Applied Crystallography*, 46(2):544–549, Apr 2013.
 - 36 Jörg Neufeind, Mikhail Feygenson, John Carruth, Ron Hoffmann, and {Kenneth K.} Chipley. The nanoscale ordered materials diffractometer nomad at the spallation neutron source sns. *Nuclear Instruments and Methods in Physics Research, Section B: Beam Interactions with Materials and Atoms*, 287:68–75, September 2012.
 - 37 S. Calder, K. An, R. Boehler, C. R. Dela Cruz, M. D. Frontzek, M. Guthrie, B. Haberl, A. Huq, S. A. J. Kimber, J. Liu, J. J. Molaison, J. Neufeind, K. Page, A. M. dos Santos, K. M. Taddei, C. Tulk, and M. G. Tucker. A suite-level review of the neutron powder diffraction instruments at oak ridge national laboratory. *Review of Scientific Instruments*, 89(9):092701, 09 2018.
 - 38 C L Farrow, P Juhas, J W Liu, D Bryndin, E S Božin, J Bloch, Th Proffen, and S J L Billinge. Pdfft2 and pdfgui: computer programs for studying nanostructure in crystals. *Journal of Physics: Condensed Matter*, 19(33):335219, jul

- 2007.
- ³⁹ Bruker. *APEX3*. Bruker AXS Inc., Madison, Wisconsin, USA, 2014.
- ⁴⁰ Lennard Krause, Regine Herbst-Irmer, George M. Sheldrick, and Dietmar Stalke. Comparison of silver and molybdenum microfocus X-ray sources for single-crystal structure determination. *Journal of Applied Crystallography*, 48(Pt 1):3–10, February 2015.
- ⁴¹ George M. Sheldrick. *SHELXT* – Integrated space-group and crystal-structure determination. *Acta Crystallographica Section A Foundations and Advances*, 71(1):3–8, January 2015.
- ⁴² George M. Sheldrick. Crystal structure refinement with SHELXL. *Acta Crystallographica. Section C, Structural Chemistry*, 71(Pt 1):3–8, January 2015.
- ⁴³ Koichi Momma and Fujio Izumi. *VESTA3* for three-dimensional visualization of crystal, volumetric and morphology data. *Journal of Applied Crystallography*, 44(6):1272–1276, Dec 2011.
- ⁴⁴ Xiangyun Qiu, Th. Proffen, J. F. Mitchell, and S. J. L. Billinge. Orbital Correlations in the Pseudocubic LaMnO_3 and Rhombohedral $\text{R}_2\text{Mn}_2\text{O}_7$ Phases of LaMnO_3 . *Physical Review Letters*, 94(17):177203, May 2005.
- ⁴⁵ Daniel P. Shoemaker, Ram Seshadri, Andrew L. Hector, Anna Llobet, Thomas Proffen, and Craig J. Fennie. Atomic displacements in the charge ice pyrochlore $\text{Bi}_2\text{Ti}_2\text{O}_6$ studied by neutron total scattering. *Phys. Rev. B*, 81:144113, Apr 2010.
- ⁴⁶ Yusuke Kousaka, Hiroyuki Ohsumi, Takashi Komesu, Taka-hisa Arima, Masaki Takata, Soichiro Sakai, Motoko Akita, Katsuya Inoue, Toshio Yokobori, Yuya Nakao, Emi Kaya, and Jun Akimitsu. Crystallographic Chirality of CsCuCl_3 Probed by Resonant Circularly-Polarized Hard X-ray Diffraction. *Journal of the Physical Society of Japan*, 78(12):123601, December 2009.
- ⁴⁷ Yusuke Inomata. Temperature-Dependent Spontaneous Resolution of CsCuCl_3 . *Crystal Growth & Design*, page acs.cgd.5c00561, July 2025.
- ⁴⁸ Yusuke Inomata, Suwan Yamada, and Tetsuya Kida. Solvent and Achiral Crystalline Phase-Induced Chiral Resolution of CsCuCl_3 . *Crystal Growth & Design*, 26(1):401–407, January 2026.
- ⁴⁹ Hiroyuki Ohsumi, Akihisa Tokuda, Soshi Takeshita, Masaki Takata, Motohiro Suzuki, Naomi Kawamura, Yusuke Kousaka, Jun Akimitsu, and Taka-hisa Arima. Three-Dimensional Near-Surface Imaging of Chirality Domains with Circularly Polarized X-rays. *Angewandte Chemie International Edition*, 52(33):8718–8721, August 2013.
- ⁵⁰ Y. Kousaka, T. Koyama, K. Ohishi, K. Kakurai, V. Hutano, H. Ohsumi, T. Arima, A. Tokuda, M. Suzuki, N. Kawamura, A. Nakao, T. Hanashima, J. Suzuki, J. Campo, Y. Miyamoto, A. Sera, K. Inoue, and J. Akimitsu. Monochiral helimagnetism in homochiral crystals of CsCuCl_3 . *Physical Review Materials*, 1(7):071402, December 2017.